NeuroImage 208 (2020) 116410

Contents lists available at ScienceDirect

NeuroImage

journal homepage: www.elsevier.com/locate/neuroimage

Low entropy map of brain oscillatory activity identifies spatially localized events: A new method for automated epilepsy focus prediction

Manel Vila-Vidal [a,*], Carmen Pérez Enríquez [b], Alessandro Principe [b,c,d], Rodrigo Rocamora [b,c,d,**], Gustavo Deco [a,e], Adrià Tauste Campo [a,***]

[a] Center for Brain and Cognition, Department of Information and Communication Technologies, Universitat Pompeu Fabra, 08005, Barcelona, Spain
[b] Hospital del Mar Medical Research Institute, 08003, Barcelona, Spain
[c] Epilepsy Monitoring Unit, Department of Neurology, Hospital del Mar, 08003, Barcelona, Spain
[d] Faculty of Health and Life Sciences, Universitat Pompeu Fabra, 08003, Barcelona, Spain
[e] Institució Catalana de Recerca i Estudis Avançats, 08010, Barcelona, Spain

ARTICLE INFO

Keywords:
Seizure onset zone
Intracranial EEG
Time-frequency analysis
Automated detection algorithms
Post-operative outcome

ABSTRACT

The spatial mapping of localized events in brain activity critically depends on the correct identification of the pattern signatures associated with those events. For instance, in the context of epilepsy research, a number of different electrophysiological patterns have been associated with epileptogenic activity. Motivated by the need to define automated seizure focus detectors, we propose a novel data-driven algorithm for the spatial identification of localized events that is based on the following rationale: the distribution of emerging oscillations during confined events across all recording sites is highly non-uniform and can be mapped using a spatial entropy function. By applying this principle to EEG recording obtained from 67 distinct seizure epochs, our method successfully identified the seizure focus on a group of ten drug-resistant temporal lobe epilepsy patients (average sensitivity: 0.94, average specificity: 0.90) together with its characteristic electrophysiological pattern signature. Cross-validation of the method outputs with postresective information revealed the consistency of our findings in long follow-up seizure-free patients. Overall, our methodology provides a reliable computational procedure that might be used as in both experimental and clinical domains to identify the neural populations undergoing an emerging functional or pathological transition.

1. Introduction

The study of high cognitive functions or brain diseases with electroencephalography often involves the identification of changes in the recorded potentials that are time-locked to an event (Luck et al., 2000; Lauchaux et al., 2012; Kropotov, 2016). Depending on the nature of the problem being addressed, this event can be the onset of an external stimulus, a motor act, or a pathological symptomatology. In all cases, the spatial localization of the changes elicited in brain activity depends on the identification of the pattern signatures of those changes.

For instance, in the context of epilepsy research and monitoring with intracranial EEG, clinicians target specific electrophysiological patterns that are known to be associated with epileptic activity. In particular, the spatial mapping of pathological patterns of activity in drug-resistant epilepsy patients undergoing pre-surgical stereo-electroencephalography (SEEG) (Talairach et al., 1974; Munari and Bancaud, 1985; Guenot et al., 2002; Engel et al., 2005) is a crucial step to delineate the seizure onset zone (SOZ) and plan a successful surgery.

Over the last decades, the problem of seizure focus localization from intracranial EEG recordings has fostered the development of quantitative tools to better characterize and understand ictal genesis and propagation. Several biomarkers characterize the epileptogenicity of the monitored brain structures based on preselected spectral features of the signal (Bartolomei et al., 2008; David et al., 2011; Gnatovsky et al., 2011, 2014;

* Corresponding author. Center for Brain and Cognition, Department of Information and Communication Technologies, Universitat Pompeu Fabra, 08005, Barcelona, Spain.
** Corresponding author. Hospital del Mar Medical Research Institute, 08003, Barcelona, Spain.
*** Corresponding author. Center for Brain and Cognition, Department of Information and Communication Technologies, Universitat Pompeu Fabra, 08005, Barcelona, Spain.
E-mail addresses: m@vila-vidal.com (M. Vila-Vidal), rrocamora@parcdesalutmar.cat (R. Rocamora), adria.tauste@gmail.com (A. Tauste Campo).

https://doi.org/10.1016/j.neuroimage.2019.116410
Received 9 July 2019; Received in revised form 7 November 2019; Accepted 26 November 2019
Available online 27 November 2019
1053-8119/© 2019 Elsevier Inc. This is an open access article under the CC BY-NC-ND license (http://creativecommons.org/licenses/by-nc-nd/4.0/).

Andrzejak et al., 2015; Vila-Vidal et al., 2017). More recent studies have proposed automatic methods based on high-frequency oscillations (HFOs) or stochastic properties of the SEEG signals in predefined frequency windows (Geertsema et al., 2015; Liu et al., 2016; Murphy et al., 2017; Varatharajah et al., 2017).

Despite many efforts, the gold standard in clinical practice still remains visual inspection of EEG recordings due a number of reasons. For instance, the heterogeneity of electrophysiological patterns associated with seizure onset (Perucca et al., 2014; Lagarde et al., 2016) represents a major drawback to design SOZ detection algorithms that are universally valid for all seizure typologies and patients. All cited works made a priori assumptions on the spectral features of ictal-driven activity (e.g. using HFOs or power in the broadband spectrum) and might turn ineffective for seizures that do not fulfil such frequency constraints. For example, SOZ detectors based on HFOs (Geertsema et al., 2015; Liu et al., 2016; Murphy et al., 2017) are very specific to fast discharges, but might overlook pathological patterns of activity dominated by lower frequency oscillations and longer temporal scales.

In the present study, we propose a novel data-driven methodology for the spatial localization of spatially confined events in brain activity from intracranial EEG recordings that makes no assumptions on the spectral properties of the pattern signatures of those events. Our method relies on finding the temporal scale and frequency range of locally enhanced neural oscillations associated with the event of interest. Central to our method is the definition of two novel measures, the global activation (GA) and the activation entropy (AE), that quantify the magnitude of spectral changes with respect to a pre-defined baseline and the spread of these activations across recording sites, respectively, at different frequencies and as time progresses from the occurrence of the event. By setting appropriate conditions on these measures, it is possible to find time-frequency windows where the most relevant sites can be optimally discriminated.

To validate our algorithm, we adjusted and applied it to peri-ictal SEEG recordings from 10 epileptic patients to identify the seizure onset patterns and localize the seizure onset zone (SOZ), achieving very high accuracy values. In the hope that it will be useful to other researchers, some of the processing tools used in this work have been publicly released as an open-access Python package (Epylib v1.0: https://github.com/mvilavidal/Epylib).

The method that we propose could be used to identify the pattern signatures and spatial localization of the brain response to events of clinical or cognitive relevance. In particular, our framework is particularly suitable to be used as a complementary tool during the pre-surgical evaluation and planning to better identify and interpret the regions involved in seizure generation and propagation.

2. Materials and methods

The method described here can be used to extract the pattern signatures (temporal and spectral features) associated to localized events of clinical or cognitive interest recorded with the use of electroencephalography techniques. Without loss of generality, our method was tested in the SOZ localization setting, where a clinically-validated benchmark is available for comparison. For the sake of simplicity, the methods' description will be referred to the case of seizure focus localization from peri-ictal SEEG recordings (Fig. 1A and B).

2.1. Low entropy map of enhanced neural oscillations

2.1.1. Magnitude and spread of enhanced oscillations: Global activation (GA) and activation entropy (AE)

The current approach builds upon the previously introduced mean activation (MA) measure (Vila-Vidal et al., 2017), which quantifies the average spectral activation of each targeted brain structure with respect to a certain baseline period for pre-defined frequency and time windows of interest (Fig. 1C). In our case, we use a pre-ictal baseline of activity (from 60 to 20 s before ictal onset). A detailed description of the computation of the MA can be found in the Supplementary Information. We will denote the MA of a given region j in the frequency band f and computed over a time window spanning from the seizure onset until time t with the following notation: $\mathrm{MA}_j(f,t)$.

For optimal focus detection we must ensure that there is a hierarchical and selective activation of SOZ contacts only. Central to our approach is the definition of two novel measures, namely the global activation (GA) and the activation entropy (AE), that are jointly optimized to find time-frequency windows of interest where ictal activity is maximal with respect to a baseline pre-ictal period and is spatially confined to a few contacts. Fig. 2 illustrates how these measures are computed and used to assess the amount of information carried in each window of interest. On one hand, the global activation (GA) quantifies the magnitude of the most relevant spectral activations with respect to the pre-ictal baseline state for a given time-frequency window of interest. It is defined as the weighted average MA over all contacts, where each contact's contribution is weighted by its own activation, thus ensuring that most active regions have a higher impact on the final value (Fig. 2A):

$$\mathrm{GA}(f,t) = \frac{\sum_{j=1}^{N} w_j * \mathrm{MA}_j(f,t)}{\sum_{j=1}^{N} w_j}, \tag{1}$$

with $w_j = \mathrm{MA}_j(f,t)$ if $\mathrm{MA}_j(f,t) > 0$, and $w_j = 0$, if $\mathrm{MA}_j(f,t) \leq 0$. On the other hand, the AE is defined as the entropy of the MA distribution and characterizes the spatial spread of spectral activations for the given time-frequency of interest. In order to compute the AE, the MA profile is first discretized using h bins homogeneously spaced between the minimum and maximum MA values, thus defining h discrete activation levels. To capture the relevant seizure dynamics, the binning needs to be adjusted to the characteristic scale of power activations associated with the ictal event. While using a large h can result in inactive channels being classified in different activation levels, a small h might be inappropriate to describe the richness of activations within a single MA profile. Based on the observed variability of seizure activations above baseline pre-ictal activity (Vila-Vidal et al., 2017), we set $h = 10$. To further validate this choice, we also ran a stability analysis varying the number of bins used to compute the AE (see Fig. 5C for results).

Probability values for each activation level (p_i for $i = 1, \ldots, h$) are found as the fraction of contacts lying within the corresponding MA bin (Fig. 2A). The Shannon's entropy of this distribution is obtained using the formula:

$$\mathrm{AE}(f,t) = -\sum_{i=1}^{h} p_i \log\left(p_i\right) \tag{2}$$

In order to systematically explore different windows for optimal SOZ detection we defined a time-frequency grid where we computed the GA and AE. To define the grid, we divided the frequency spectrum into a set of non-overlapping bands and considered a set of nested time windows obtained by fixing the left bound at seizure onset and varying the right bound. The granularity of the exploration grid can be tuned depending on the properties of the changes that need to be detected. We adjusted our choice to appropriately capture the characteristic spectral properties of seizure onset patterns that are typically found in clinical practice and described in the literature (Perucca et al., 2014; Lagarde et al., 2016). Specifically, we split the frequency spectrum into 10 bands defined by the following cutting-points: 1, 4.2, 8, 12, 31, 50, 73, 88, 107, 130 and 150 Hz. In the time-domain, we considered windows with right bound from 100 ms to 30 s after seizure onset using a finer granularity in the vicinity of seizure onset in order to account for fast short-lasting activity (steps of 100 ms from 100 ms to 5 s and steps of 1 s from 5 to 30 s). Additionally, we also considered time windows spanning from seizure onset into the pre-ictal period, i.e., with right bound at seizure onset and left bound ranging from 30 s to 0.1 s before seizure onset, with the same spacing as before.

For each time-frequency window in the exploration grid, we computed the MA profile and extracted its GA and AE. Fig. 2B and C shows the GA and AE distributions for one exemplary seizure, respectively.

2.1.2. Pattern signature and spatial map of localized emerging oscillations

Fig. 3 summarizes the processing steps to obtain the optimal time-frequency windows for SOZ detection (referred to as seizure onset windows, SOWs) and the SOZ. SEEG signals in the peri-ictal period were band-pass filtered in pre-defined bands of interest spanning the whole spectrum (Fig. 3A). For each band, MAs were obtained for all possible time windows of interest (Fig. 3B). For each time-frequency window in the exploration grid, we extracted the GA and AE from the MA distribution as described in the previous section (Fig. 3C).

Seizure onset window (SOW) detection was achieved by finding time-frequency windows that maximized the GA under the constraint of low AE to ensure that spectral activations were confined only to a few contacts. We considered all pairs (f,t) with positive times (i.e., excluding time windows in the pre-ictal state) and set two threshold conditions, one per variable. Regarding the first variable, we restricted our analysis to the right tail of the GA distribution, primarily selecting the 5% of the windows with the highest GA values. We further required GA to be above 3 to

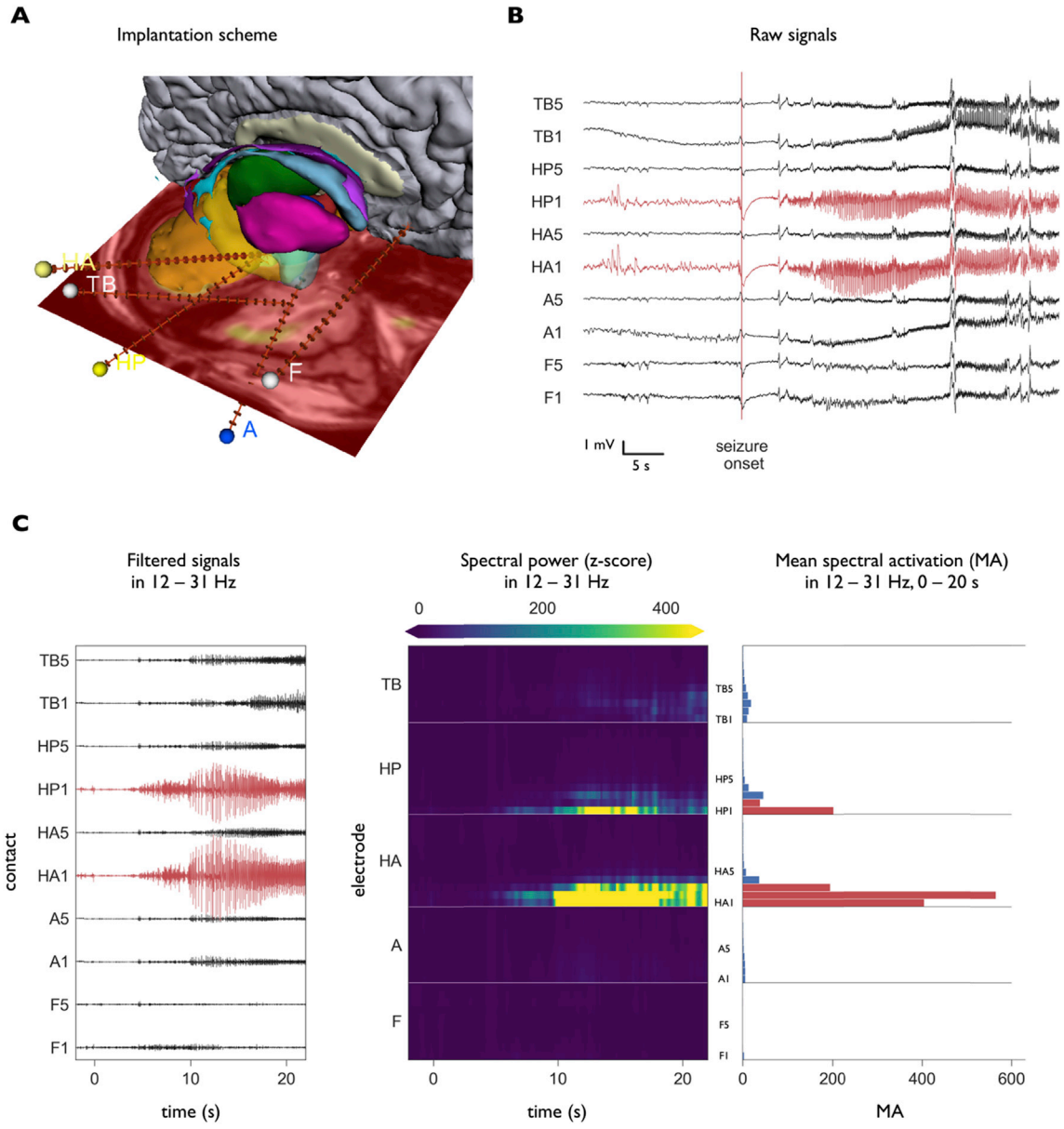

Fig. 1. Example of SEEG signal analysis for a time window (0–20 s after seizure onset) and frequency band of interest (12–31 Hz) in a seizure of patient 1. **(A)** Medial view of the brain showing the trajectories of the five electrodes and their target regions. Electrode labels refer to the regions monitored by their internal contacts: lateral parts of the orbitofrontal cortex (F), amygdala (A), anterior hippocampus (HA), posterior hippocampus (HP) and temporal pole (TB). Contacts within an electrode are numbered starting from inside. Contacts HA1, HA2, HA3, HP1 and HP2 were identified as being part of the seizure onset zone in the pre-surgical evaluation. **(B)** SEEG recordings from a selection of contacts (two per electrode) around the seizure onset (20 s of pre-ictal and 40 s of the seizure period are shown). Clinically identified SOZ contacts are marked in red. **(C)** Signal analysis in a given time window (0–20 s after seizure onset) and frequency band (12–31 Hz) of interest. Signals were first band-pass filtered at 12–31 Hz and the first 20 s of ictal activity were selected for analysis (left). Each contacts' instantaneous spectral power was obtained using the Hilbert transform method and z-scored with respect to a baseline distribution defined by accumulating the power values of all contacts during the first 40 s of the pre-ictal period (middle). The mean activation (MA) was computed for each contact by averaging all power values in the first 20 s of the ictal period (right).

ensure significant global activations with respect to the pre-ictal state. Additionally, we set a threshold of 0.5 on the AE, selecting windows with entropies smaller than this value. The decision to choose this value was based on a theoretical property of the entropy function that we derived (see Supplementary Information) to find lower bound estimates on the fraction of inactive channels induced by the AE threshold. As an example, if a time-frequency window has an AE smaller than 0.5, at least 80% of the recording sites must be in the same activation level (i.e., they must lie within the same MA bin). In addition to the primary threshold values (GA>95th percentile, AE<0.5), we performed a stability analysis to show the robustness of the methods' output with respect to particular threshold choices (see Fig. 5B for results).

All time-frequency windows satisfying both threshold conditions were preselected as candidates to be SOWs. Finally, for each frequency band we kept only the first set of consecutive time windows fulfilling the required criteria. Fig. 3D shows the selected SOWs for an exemplary seizure. For each SOW, we identified the highly populated low-activation bin. Then, contacts in higher activation levels were considered to be part of the SOZ (Fig. 3E). This procedure was repeated for all selected SOWs, and SOZ contacts were accumulated, thus obtaining a single SOZ per seizure (Fig. 3F). Tuning the parameter values (number of activation levels, GA threshold and AE threshold), the method described in this section can be adapted to alternative settings to localize the focus of spatially confined events in brain activity (the SOZ in the epileptic seizure scenario) and to extract the temporal and spectral features of those events (the SOWs in the epileptic seizure scenario).

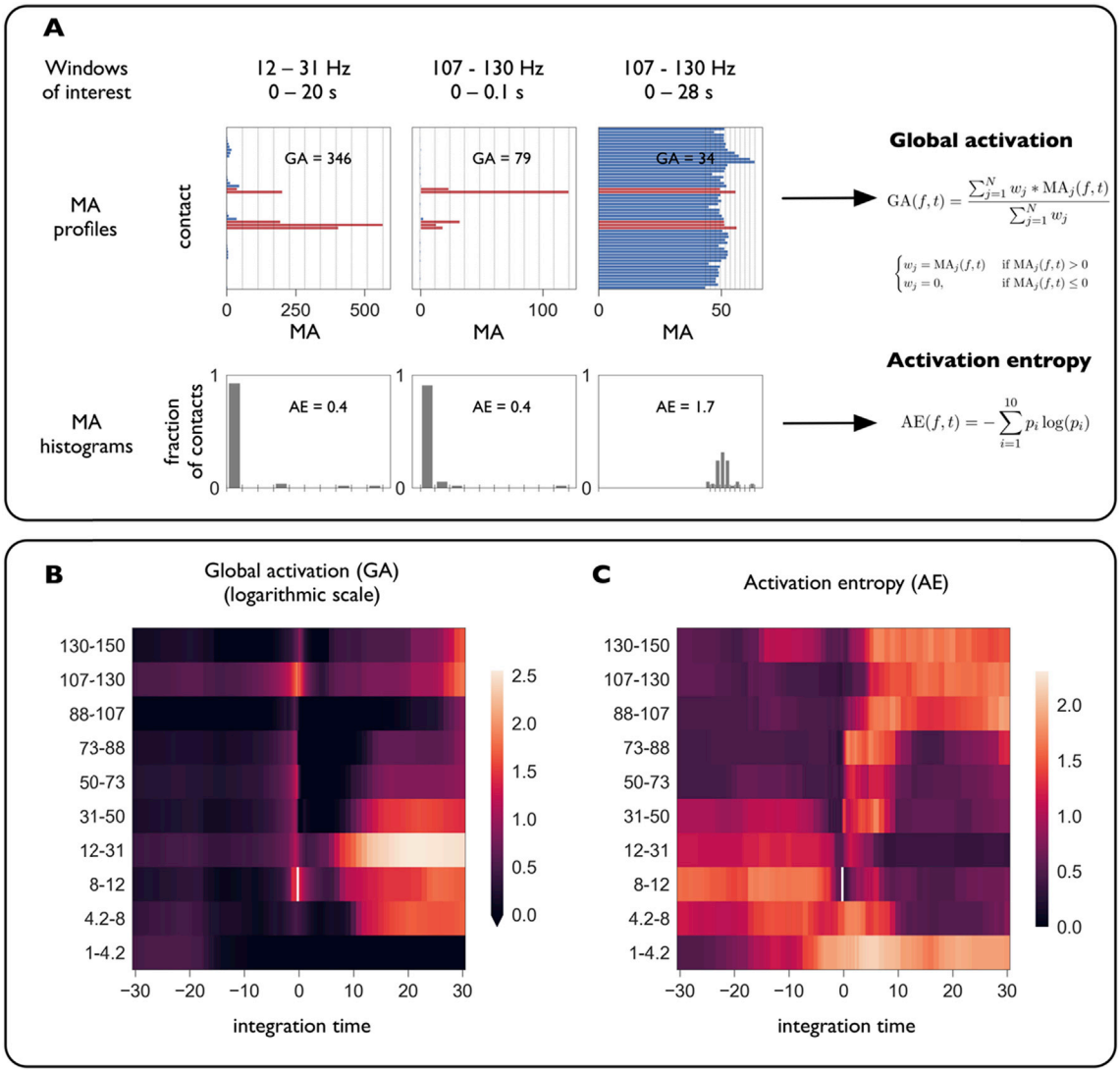

Fig. 2. Two novel measures characterize the magnitude and spread of enhanced neural oscillations. Exploration of spectral activations in different frequency and time windows of interest is done around seizure onset. **(A)** MA profiles (mean spectral activation) and MA histograms (with h = 10 bins) for an exemplary selection of windows of interest. Visually marked SOZ channels are shown in red. The first two time-frequency windows (12–31 Hz, 0–20 s; 107–130 Hz, 0–100 ms) result in very structured and selective activations of SOZ channels. The third example (107–130 Hz, 0–28 s) shows a uniform channel activation, indicating that averaged high-frequency activity is present in all recording sites. Two measures characterize the suitability of a given time-frequency window for SOZ detection. The global activation (GA) quantifies the magnitude of the highest activations for a given frequency and time window. It is defined as the weighted average MA over contacts, where each contact's contribution is weighted by its MA value (most active channels have a higher impact on the final value). The activation entropy (AE) quantifies how spread spectral activations are across recording sites. It is obtained by computing the Shannon's entropy of the MA histogram with h bins homogeneously spaced between the minimum and maximum MA values (here we use h = 10). Lower entropies of the MA distribution indicate structured and spatially confined spectral activations, whereas higher values indicate distributed and spatially extended activations. **(B)** Global activation (GA) across all possible combinations of time and frequency windows of interest in the peri-ictal period. Positive and negative times denote time windows spanning from seizure onset into the ictal and pre-ictal epochs, respectively. **(C)** Activation entropy (AE) across all possible combinations of time and frequency windows of interest in the peri-ictal period.

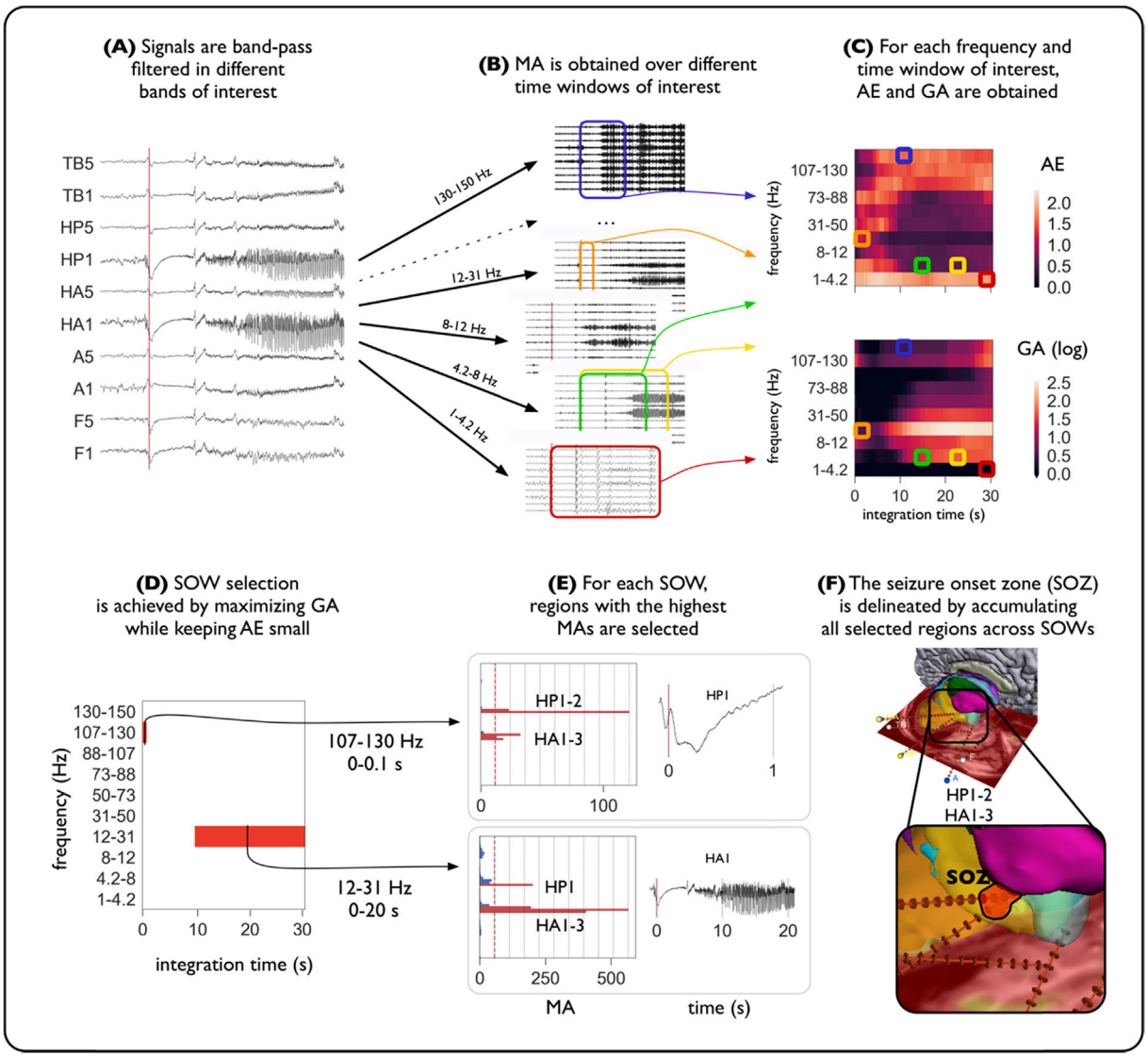

Fig. 3. Processing steps from SEEG broadband signals to SOZ detection. Identification of the most relevant seizure onset windows (SOW) and seizure onset zone (SOZ) detection is illustrated with a seizure of patient 1. **(A)** Signals are band-pass filtered in pre-defined bands of interest spanning the whole spectrum. **(B)** The mean spectral activation (MA) is obtained over different time windows and frequencies of interest using the Hilbert transform method and averaging instantaneous spectral activations across time. **(C)** For each time-frequency window, the MA profile is characterized by two summary measures: the global activation (GA) and the activation entropy (AE). **(D)** SOW detection is achieved by finding time-frequency windows that maximize GA under the constraint of low AE. Frequencies and time windows for which GA is above the 95th percentile and the AE is below 0.5 are selected. Selected time-frequency windows are marked in red. **(E)** For each seizure onset window, we identified the highly populated low-activation bin. Then, contacts in higher activation levels were considered to be part of the SOZ (AE-induced threshold marked with a dotted red line). Active regions are marked in red in the bar plots. **(F)** Active regions are accumulated across all SOWs, thus obtaining a single SOZ (shaded in red) for each seizure.

2.2. Clinical applications

2.2.1. Ethics statement

All diagnostic and surgical procedures have been previously approved by The Clinical Ethical Committee of Hospital del Mar (Barcelona, Spain).

2.2.2. Patient selection

We selected ten patients with pharmacoresistant temporal lobe epilepsy that underwent stereo-EEG in the Epilepsy Monitoring Unit of Hospital del Mar (Barcelona, Spain). Patient inclusion was based on the following criteria: (a) that the seizure focus had been identified by the epileptologists and (b) that ictal onset was confined to a reduced number of contacts corresponding to an anatomical region. Demographic and clinical information for all patients is summarized in Table 1. The decision to implant depth electrodes, the decision of the targeted areas and the implantation duration were based solely on clinical grounds and independent of this study.

2.2.3. SEEG recordings

Recordings were obtained using 5 to 21 intracerebral multiple contact microelectrodes (Dixi Medical, Besançon, France; diameter: 0.8 mm; 5 to 15 contacts, 2 mm long, 1.5 mm apart) that were stereotactically implanted using robotic guidance (ROSA, Medtech Surgical, Inc). Between 56 and 126 contacts were implanted and recorded in each subject. Fig. 1A shows the implantation scheme of patient 1. Signals were recorded using a standard clinical EEG system (XLTEK, subsidiary of Natus Medical) with 500 Hz of sampling rate, except for patient 3, where a sampling rate of 250 Hz was used (Fig. 1B). SEEG recordings from a

Table 1
Main data of patients included in the study.

Patient	Gender/ Age	Epilepsy	Side	Duration (years)	Electrodes (left)	Number of recording sites	Number of sites within the SOZ	Analyzed seizures	MRI	Surgery	Treated structure	Outcome (Engel's class)	Follow-up (years)
1	F/27	TLE	R	10	5(0)	54	5	8	negative	R TATL	Temporal pole, amygdala and head of hippocampus	Ia	6
2	F/30	TLE	L	25	7(7)	67	9	8	negative	SAH	temporal pole, inferior half of amygdala and anterior 1/3 of hippocampus	Ic	6
3	F/55	TLE	L	40	6(6)	59	6	1	negative	L TATL	temporal pole, amygdala and head of hippocampus	Ib	6
4	M/29	TLE	R	9	0(0)	95	11	8	negative	NO		Ia	5
*5	M/43	TLE	R	42	15(0)	125	3	5	FCDIIIa. Arachnoid Cyst.	R TATL	temporal pole, amygdala and 2/3 of hippocampus	Ia	3
6	M/26	TLE	R	11	7(0)	78	11	7	R amygdala enlargement	RF-TC	temporal pole, amygdala, entorhinal cortex and fusiform gyrus	Rp (Ib)	4
7	M/20	TLE	L	12	15(15)	122	6	7	negative	RF-TC	anterior and posterior superior temporal gyrus, transverse temporal gyrus and supramarginal gyrus	Rp (Ib)	4
8	M/40	TLE	L	2	8(8)	85	5	7	L temporal polar blurring	RF-TC	temporal pole and hippocampal head	uRp (III)	4
9	F/52	TLE	L	45	10(8)	104	8	6	gliosis near R craniotomy	L TATL	temporal pole, inferior half of amygdala and anterior 1/3 of hippocampus	Ib	5
10	F/40	TLE	L	16	10(8)	107	14	10	L posterior hippocampal lesion	L TATL	2/3 of amygdala, anterior 2/3 of hippocampus	III	6

F = female; M = male; TLE = temporal lobe epilepsy; R = right; L = left; FC = frontal cingulate; R FC = right frontal cingulate; L FC = left frontal cingulate; A = amygdala; Ha = anterior hippocampus; Hp = posterior hippocampus; TP = temporal pole; EC = entorhinal cortex, OFCm = mesial orbitofrontal cortex; TGi = inferior temporal gyrus; PHCp = posterior parahippocampal cortex; W=Wernicke's area; TOJ = temporal occipital junction; FBC = frontal basal cortex; MS = motor strip; TCl = lateral temporal cortex; OCm = mesial occipital cortex; FS = focal seizure; w = with; wo = without; CA = consciousness alteration; TATL: Tailored anterior temporal lobectomy; RF-TC = Radiofrequency thermocoagulation; SAH=Selective amygdalohyppocampectomy; Rp = Responsive; uRp = Unresponsive; NO = not-operated. *Patient 5 was initially responsive to RF-TC, but experienced seizure relapse two years after the procedure. He then underwent resective surgery, after which achieved seizure freedom (Engel I) with a follow-up of 3 years.

total of 67 spontaneous seizures were collected and analyzed. Seizure onset and termination times of each seizure were independently marked by two epileptologists (A.P. and R.R.) and a consensus decision was reached. For each seizure we selected the marked ictal epoch together with 60 s of pre-ictal baseline activity. Artifacted channels were identified by visual inspection and removed prior to data analysis. SEEG signals were primarily analyzed in the referential recording montage. A broadband-pass filter (FIR, filter band [1,165] Hz) was used to remove slow drifts and aliasing effects. We also used a notch FIR filter at 50 Hz and its harmonic frequencies to remove the power line interference.

2.2.4. Clinical benchmark: Seizure onset zone and post-surgical outcome

After electrode implantation and monitoring, SOZ was identified two epileptologists (A.P. and R.R.) using visual inspection (percent inter-rater agreement of 0.97 and Cohen's kappa score of 0.80, with N = 906 total recording sites). For our study, we selected sites that were identified at least by one of the two epileptologists. In each patient, ictal activity was found to start in 3–14 channels that were marked as being part of the SOZ. In total, 78 recording sites were defined as the SOZ across patients, which accounts for 9% of the 906 implanted contacts. Surgical resection or radio-frequency thermocoagulation (RF-TC) was planned based on individual SEEG evaluations. At the time of submission (June 2019), Patients 1–3 had achieved seizure freedom after surgical resection (Engel I) with a follow-up period of 6 years. Patient 4 achieved seizure freedom after electrode explantation without need of resective surgery (Engel I) with a follow-up of 5 years. Patient 5 was initially responsive to RF-TC (Bourdillon et al., 2017), but after seizure relapse underwent resective surgery, after which achieved seizure freedom (Engel I) with a follow-up of 3 years. Patients 6, 7 and 8 underwent only RF-TC. Patients 6 and 7 are seizure free (Engel I) with a follow-up of 3 years. Patient 8 was initially responsive to RF-TC showing a seizure reduction larger than 50%, but relapse occurred 2 years after the procedure. Resective surgery was not an option for this patient due to cognitive risks. Patient 9 achieved seizure freedom after surgical resection (Engel I) with a follow-up period of 5 years. We also included one patient (patient 10) in which the outcome was not successful (Engel III) because the brain resectomy failed to completely remove the identified seizure focus.

2.2.5. Method validation: Statistical and stability analysis

We used our algorithm to obtain the SOZ contacts in each seizure separately. For each patient, the SOZ was defined by accumulating all seizure-specific detected SOZ regions (Supplementary Fig. 2A). In order to assess the performance of our method, we compared the SOZ given by the algorithm with the SOZ marked by epileptologists during diagnosis (clinical benchmark). For each patient, we computed the sensitivity and specificity of the algorithm output (Supplementary Fig. 2B; see Fig. 5A for results). In order to quantify the localization error, we computed the spatial distance between missed SOZ contacts (false negatives) and the SOZ delineated by our method (Supplementary Fig. 2C).

Then, we ran a stability analysis to assess the dependence of the results on the parameters of the algorithm and to validate our parameter choices (number of activation levels used to discretize the MA profile h = 10, GA threshold = 95th percentile, AE threshold = 0.5). On one hand, we studied the effect of the GA and AE thresholds by computing the accuracy of the method as the threshold values were varied (see Fig. 5B for results). Dependence on the two thresholds was tested independently of each other. Specifically, we computed the sensitivity and the specificity of the method as a function of the GA threshold (from 0 to 100) with AE fixed around its primary value (0.5). For each value of the GA threshold, we ran the algorithm multiple times (AE threshold values in the range 0.4–0.6, step = 0.01, N = 20) and computed the average and the standard deviation of the sensitivity and specificity across the different runs. The same procedure was repeated to assess the performance as a function of the AE threshold, while keeping the GA threshold fixed around its primary value (95). For each value of the AE threshold, we ran the algorithm multiple times (GA threshold values in the range 92–98, step = 1, N = 6) and computed the distribution of accuracies across runs. On the other hand, we assessed the effect of the binning of the MA profile on the method performance (see Fig. 5C for results). Specifically, we computed the sensitivity and specificity of the method as a function of the number of bins used to compute the AE quantifier (see equation (2)).

This procedure was primarily done with SEEG signals in the monopolar configuration and with positive times (ictal period). We then compared the accuracy of the SOZ detection algorithm under different recording configurations (monopolar vs. bipolar) and time periods (ictal vs. pre-ictal) (see Fig. 6 for results). In order to avoid confounders introduced by the threshold choices, we computed the accuracy (sensitivity, specificity) curves of the algorithm as a function of the threshold values in each case separately. Then, we extracted and compared the area under the curve (AUC) across conditions as a threshold-independent measure of the method performance.

Finally, to relate the results of our method with validated post-operative information, we subselected patients (N = 5) that underwent resective surgery and had an Engel I post-surgical outcome (see Fig. 7 for results). For this subset of patients, we defined three regions of interest: (a) the seizure onset zone (SOZ), (b) the resected zone (RZ), consisting of all recording sites that were surgically ablated, and (c) the union of the two previous regions, consisting of all SOZ and/or RZ sites (SOZ + RZ) and therefore representing all putative sites with a critical role in the generation and/or spread of the patients' seizure. For each of these regions of interest, we assessed the prediction power of the variable MA when considered only in seizure onset windows. In particular, we first normalized the MA values within each SOW to allow for cross-window comparison. For each patient, we averaged all normalized MA values across all SOWs of all seizures, thus defining a single normalized MA index (nMA) per patient's site. By setting a cutoff value on the nMA index, we defined a binary classifier that was then compared to each region of interest. In each case, the predictive value of the classifier was assessed by extracting the area under the curve (AUC) per patient.

2.2.6. Seizure onset time detection with continuous GA

Although out of this work's main scope, we wished to assess whether our novel quantifier GA could be used to automatically identify seizure onset times. To do so, we used a continuous version of GA in the broadband spectrum combined with the Page-Hinkley algorithm (Page, 1954; Hinkley, 1971) for detecting change-points in random quantities (see Supplementary Information for details on the algorithm and how we set its parameter values). For each patient, we computed the fraction of seizures in which the algorithm yielded a detection time and we quantified the distance between the onset times given by clinicians and the onset time detected by the algorithm (see Supplementary Fig. 6 for results).

2.3. Data and code availability

Due to institutional restrictions, the data that supports the findings of this study can be accessed only with a data sharing agreement. The code used in this study is available from the corresponding author upon request. Some processing tools used in this work have been publicly released as an open-access Python package (Epylib v1.0: https://github.com/mvilavidal/Epylib).

3. Results

3.1. Locally enhanced oscillations in the transition from pre-ictal to ictal dynamics

In all studied patients and seizures, we computed all channels' MA activation in the preselected frequencies and time windows of interest and extracted the GA and AE from the MA profiles. We first studied the extent to which both variables were providing redundant information.

For each seizure, we computed the Spearman correlation coefficients between the two variables. This computation yielded small-medium correlation values (Spearman's r = −0.4 ± 0.3, mean ± standard deviation across N = 67 seizures, 91% of significant outcomes after correction for multiple comparisons at the familywise error rate of 0.01, see Supplementary Table S1), confirming that both variables were providing non-redundant information.

In this stage, we sought to characterize differences between the pre-ictal and ictal periods arising in the joint (AE,GA) empirical distribution at the group level (see Supplementary Information for details). To this aim, we normalized all GA values using the percentile score in each seizure and period (ictal, pre-ictal) and pooled all (AE,GA) values across seizures. A large number of ictal windows were found to cluster in the region with GA>80 and AE<0.5 (Supplementary Fig. 3A). On the other hand, pre-ictal windows exhibited a more sparse distribution of (AE,GA) values, with an average trend of higher AEs and lower GAs (Supplementary Fig. 3B). In particular, the region used for SOW detection in this study was GA>95 and AE<0.5 (See Materials and Methods). Then, for each seizure included in the study (a total of N = 67) we compared the fraction of time-frequency windows satisfying both conditions with chance level (see the Supplementary Information for details). In both periods, the fraction of windows with GA>95 and AE<0.5 was found to be significantly above chance level (Supplementary Fig. 4), being this trend higher in the ictal period. Hence, we hypothesize that this association between very high and spatially confined activations is associated with ictal onset and constitutes an *a posteriori* validation of the rationale behind the procedure that we propose.

3.2. Seizure onset window detection

In 88% of the analyzed seizures (59 out of 67) the method was able to identify time-frequency windows satisfying the required criteria on the magnitudes of the variables GA and AE. In the remaining eight seizures no window fulfilled the conditions due to a number of reasons, including low spectral activations below the minimum required threshold of 3 standard deviations with respect to the pre-ictal baseline (1 seizure), widespread simultaneous activations that did not allow for a confined region to be safely identified (five seizures) or large pre-ictal activations comparable to the ictal activity itself (two seizures). The latter was the case of patient 5. Reviewing of the SEEG recordings from the two discarded seizures revealed that ictal onset was indeed preceded by continuous ictal-like activity.

3.3. Seizure onset windows unveil characteristic electrophysiological signatures

In each seizure, the SOWs were qualitatively found to pinpoint the characteristic frequency and time windows of the seizure onset patterns. As an example, in the first seizure of patient 1, the algorithm selected the following SOWs: 107–130 Hz during the first hundreds of milliseconds and 12–31 Hz between 10 and 20 s. Regions of the posterior and anterior hippocampi were selected as being inside the SOZ. Inspection of the electrophysiological activity recorded around seizure onset revealed that the output of the method was qualitatively describing the seizure onset patterns (Fig. 4A).

SOWs were found to be heterogeneous across patients and, in some cases, even across seizures of the same patient. For each time-frequency window of interest, we computed the fraction of seizures for which that window was a SOW (Supplementary Fig. 5). The most common SOWs were found to be in the frequency range 12–31 Hz with end times spanning from 10 to 30 s after seizure onset. These SOWs were found in approximately 50% of all analyzed seizures, corresponding to low-voltage fast-activity (LVFA) combined with rhythmic spikes (RS), as seen in the first seizure of patient 1. These were followed by SOWs corresponding to slower activity at 8–12 Hz, appearing in approximately 25% of the seizures. Of particular interest was the SOW at 107–130 Hz during the first milliseconds after seizure onset, appearing in around 15% of the seizures, which is consistent with the literature about HFOs being a good biomarker of pathological epileptic activity (Murphy et al., 2017).

Additionally, for each patient and frequency of interest, we computed the fraction of seizures in which that particular frequency appeared to be part of the SOW. Roughly, three different frequency distributions could be identified within our cohort. Fig. 4B shows these distributions for three exemplary cases and the seizure onset patterns they correspond to as described in (Lagarde et al., 2016). In patient 1 the most relevant frequencies were found to be between 4.2 and 12 Hz. In this case, seizure onset is characterized by LVFA + RS activity that becomes particularly visible around 10 s after seizure onset. In some cases, fast discharges (between 110 and 150 Hz) have also a role during the first milliseconds of the ictal period, while in others rhythmic slow waves (RSWs) in the θ band (4–8 Hz) can be observed. Seizure onset in patient 5 was found to be characterized by very slow spiking activity (~1 Hz) of large amplitude in between 10 and 20 s after seizure onset, that becomes faster (up to ~4–8 Hz) as the seizure progresses. Patient 6 exhibited a much more spectrally diffuse activity (ranging from 50 to 150 Hz in most seizures) of very low amplitude that becomes sufficiently high for SOZ discrimination around 20 s after seizure onset.

3.4. Seizure focus prediction

Patient specific sensitivities and specificities are reported in Fig. 5. The average sensitivity of the method across patients was 0.94 ± 0.03 (mean ± standard error of the mean), with an average specificity of 0.90 ± 0.03 (mean ± standard error of the mean). In patients 1, 3, 5, 7, 8, 9 and 10 all SOZ regions were identified by our method (sensitivity = 1). In the remaining cases (patients 2, 4 and 6) false negatives (SOZ contacts mistakenly marked as non-epileptogenic) lied at most 1 contact (i.e. 1.5 mm) apart from true positives (regions correctly marked as epileptogenic).

3.5. Stability analysis

Results of the stability analysis with respect to the GA and AE thresholds are shown in Fig. 5B. The threshold choice was found to have a small effect on the specificity values (above 0.7 for all threshold values). The primary value used for the GA threshold (95th percentile) was found to lie at the onset of the sensitivity function stabilization, yielding an optimal trade-off between sensitivity and specific. On the other hand, the AE threshold (0.5) was found to lie on a plateau of the performance functions. These results confirm the validity of the theoretical derivations behind our value choices.

The effect of the number of activation levels used to compute the AE quantifier is shown in Fig. 5C. This parameter was found to have a major impact on the sensitivity of the algorithm. Its selected value (10) was found to lie on a plateau of sensitivity, thus confirming our hypothesis that our choice captures the richness of channel's MA distribution upon seizure onset.

3.6. Comparative performance between monopolar and bipolar configurations

SOZ detection and stability analysis were primarily done with SEEG signals in the monopolar configuration. The whole analysis was then repeated using the bipolar configuration. In order to compare the level of performance in the two settings independent of the selected algorithm working point, we computed the patient-average sensitivity and specificity curves as a function of the thresholds in each configuration and compared their AUCs (Fig. 6A). No relevant differences were found in terms of specificity. Conversely, the algorithm was found to be significantly more sensitive to SOZ regions in the monopolar configuration. In particular, the relative AUC of the sensitivity as a

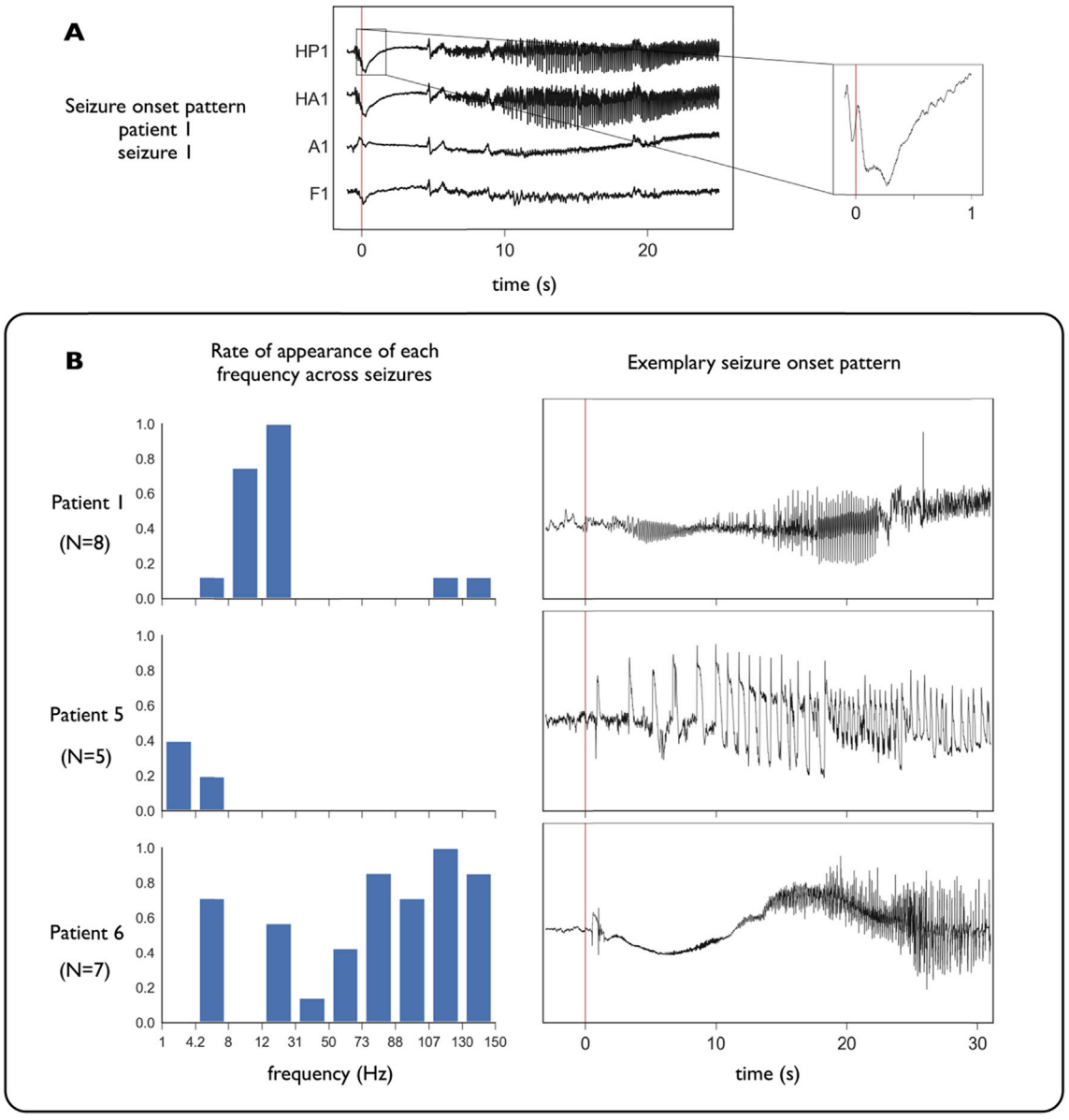

Fig. 4. Seizure onset windows unveil epileptogenic pattern signatures. **(A)** Detail of the seizure onset pattern in a seizure of patient 1. We show electrophysiological activity recorded at two SOZ contacts (HP1, HA1) and two contacts outside the SOZ (A1, F1). Seizure onset is marked with a red vertical line. As suggested in Fig. 3, the seizure is initiated at a hippocampal level with rapid discharges (~110 Hz) of very low amplitude in the first hundreds of milliseconds that are particularly clear in HP1. This activity is followed by low-voltage fast-activity (LVFA) at 12–31 Hz that becomes visible 5 s after seizure onset and that increases in amplitude as the seizure progresses. Activations observed at 12–31 Hz are in fact a combined effect of LVFA activity (~30 Hz) together with slow rhythmic spikes (RS) (~15 Hz) of high amplitude particularly observable between 10 and 20 s. This activity then propagates into other regions and is no longer specific to SOZ regions (not shown). **(B)** Seizure onset frequencies along with their corresponding seizure onset patterns for three representative patients with 8, 5 and 7 seizures, respectively. (Left) For each patient and frequency of interest, the bar height indicates the fraction of seizures in which the frequency appeared in at least one SOW. (Right) In each case, we show the electrophysiological pattern recorded at an exemplary SOZ site after seizure onset for a given seizure. Seizure onset is marked with a red vertical line. In patient 1 seizures typically start with LVFA (~30 Hz) combined with RS (~10 Hz). In the example, rhythmic slow waves (RSWs) in the θ band (4–8 Hz) are also observed. In patient 5 seizure onset is characterized by very slow spiking activity (~1 Hz) of large amplitude that becomes faster (up to ~4 Hz) as the seizure progresses. Patient 6 has a much more spectrally diffuse activity (50–150 Hz) of very low amplitude. As seen in the example, there is also a very slow wave or baseline shift that was not detected by our method.

function of the GA threshold was found to be 0.98 ± 0.01 in the monopolar configuration, while it dropped to 0.84 ± 0.01 in the bipolar configuration (mean ± standard deviation across different runs of the algorithm with AE fixed in the range 0.4–0.6). On the other hand, while varying the AE threshold the relative AUC of the sensitivity was 0.85 ± 0.02 in the monopolar configuration and 0.70 ± 0.03 in the bipolar setting (mean ± standard deviation across different runs of the algorithm with GA fixed in the range 92–98).

3.7. Focus prediction in the pre-ictal period

Additionally, we assessed the amount of SOZ predictability carried in the pre-ictal activity. We repeated the same analysis described in the previous sections using pre-ictal time windows (i.e., negative times from −30 to 0 s) in the monopolar setting. With the primary values of the thresholds, the patient-average sensitivity and specificity of SOZ localization in the pre-ictal period were lower than in the ictal period: 0.8 ± 0.1 and 0.77 ± 0.04 (mean ± standard error of the mean across patients),

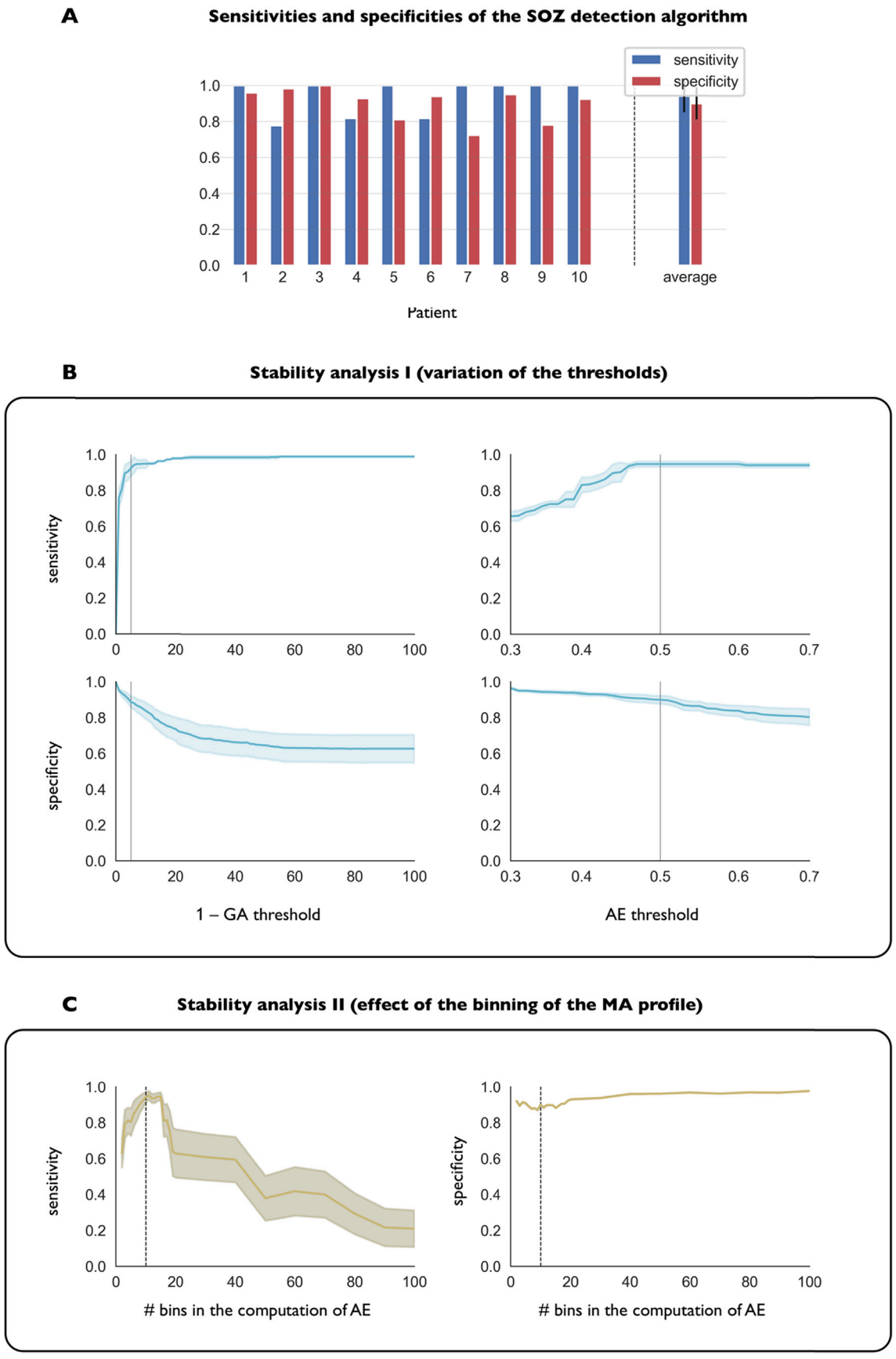

(caption on next page)

Fig. 5. Validation of the method: SOZ detection accuracy and stability analysis. **(A)** Performance of the SOZ detection algorithm. In each patient, we localized the SOZ using our algorithm and compared the classification given by the algorithm with the clinical benchmark provided by clinicians. The figure reports sensitivities and specificities at the subject and group levels. The average sensitivity of the method across patients was 0.94 ± 0.03 (mean ± standard error of the mean). The average specificity was 0.90 ± 0.03 (mean ± standard error of the mean). Only in patients 2, 4 and 6 the identification was not complete. However, false negatives (SOZ contacts mistakenly marked as non-epileptogenic) lied at most 1 contact (i.e. 1.5 mm) apart from true positives (regions correctly marked as being inside the SOZ). **(B)** Stability analysis I (variation of the thresholds). The figures show the patient-average accuracy of the SOZ detection algorithm as a function of the two threshold conditions (GA and AE). (Left) Accuracy (sensitivity and specificity) of the detection algorithm as a function of the GA threshold when AE is fixed around 0.5. For each value of the GA threshold, we ran the algorithm multiple times (AE threshold values in the range 0.4–0.6, step = 0.01, N = 20 runs). The solid lines and shaded areas represent the average accuracy and its standard deviation, respectively, across the different runs. (Right) Accuracy (sensitivity and specificity) of the detection algorithm as a function of the AE threshold when GA is fixed around 95. For each value of the AE threshold, we ran the algorithm multiple times (GA threshold values in the range 92–98, step = 1, N = 6). The solid lines and shaded areas represent the average accuracy and its standard deviation, respectively, across the different runs. Vertical lines mark the working point of the algorithm in our study (GA and AE thresholds set at 95th percentile and 0.5, respectively), for which the algorithm attains high accuracy values. **(C)** Stability analysis II (effect of the binning of the MA profile). Patient-average accuracy (sensitivity and specificity) of the SOZ detection algorithm as a function of the number of bins used to compute the AE quantifier (see equation (2)). The solid lines and shaded areas represent the average accuracy and its standard deviation, respectively, across different patients. The vertical lines indicate the actual number of bins used in this study (h = 10), for which the algorithm attains high accuracy values.

respectively. Comparison of AUCs of the accuracy curves as the thresholds were varied yielded the same results (Fig. 6B).

3.8. Method validation with post-surgical outcome

For patients that underwent resective surgery and had a very good post-surgical outcome (Engel I, N = 5), the binary classifier induced by nMA indices in the SOWs selected by the algorithm was compared across the three regions of interest (SOZ, SOZ + RZ and RZ). ROC curves for each region of interest are shown in Fig. 7. SOZ prediction achieved very high AUC values: 0.997 ± 0.001 (mean ± standard error of the mean). When compared to RZ + SOZ and RZ, the classifier achieved lower but still notable predictive power values (0.79 ± 0.05 and 0.69 ± 0.08, respectively), indicating that the nMA variable carries relevant information not only for SOZ identification, but also for RZ prediction.

3.9. Seizure onset time detection with continuous GA

The results of seizure onset detection with the Page-Hinkley algorithm combined with the continuous version of GA are shown in Supplementary Fig. S6. For patients 1–8, the Page-Hinkley algorithm performed very well, yielding detection times in 96% of N = 51 seizures with an average time lag of 2 ± 7 s (mean ± standard deviation across N = 51 seizures) with respect to the seizure onset time provided by epileptologists. Seizure onset detection was very poor in patient 9 (detection times found in 5 of 6 seizures with an average delay of 60 ± 30 s, mean ± standard deviation across N = 5 seizures). In patient 10, detection times were found only in 3 of 10 seizures with an average delay of 47 ± 30 s (mean ± standard deviation across N = 10 seizures). Results were stable across different values of the algorithm parameters in most cases (patients 1–9). In patient 10, the low performance of the algorithm was due to activations of low magnitude upon seizure onset that could be detected by relaxing the detection conditions. Optimization of the algorithm parameters for this particular case yielded better detection times (average time lag of 0 ± 21 s, mean ± standard deviation across N = 10 seizures).

4. Discussion

We proposed a novel methodology to automatically estimate the localization of spatially confined events in brain activity using the low entropy properties of emerging neural oscillations associated to those events. Our analysis was motivated by the problem of SOZ identification from intracranial EEG signals in patients with pharmacoresistant epilepsy. In this context, spatially confined activations with respect to a pre-ictal baseline were taken as signatures of epileptogenic tissue and were used to localize the seizure focus. We tested the algorithm's performance on a group of ten patients with varied seizure onset patterns and follow-up periods that range from 3 to 6 years. In each case, the underlying time-frequency windows were found to pinpoint the characteristic spectral features (frequency and duration) of onset patterns. Additionally, we were able to relate our findings with the postsurgical information of patients that attained seizure freedom after resective surgery using the core measure of the study as a putative predictor of the resected zone.

4.1. The global activation (GA) and activation entropy (AE) capture landmarking features of seizure initiation

Based on previous studies (Bartolomei et al., 2008; David et al., 2011) we defined ictal-driven activity as an increase in signal power from pre-ictal to ictal epochs. In particular, we used the mean activation (MA) measure (Vila-Vidal et al., 2017), which quantifies the average spectral activation of each targeted brain structure for pre-defined frequency and time windows of interest (Fig. 1). However, while most studies constrained spectral activations to occur in preselected frequency bands, our method automatically infers the characteristic temporal scale and frequency range of locally enhanced oscillations in each case, thus maximizing the amount of information relevant for SOZ detection in a patient and seizure-specific context. Hence, by avoiding such frequency constraints, the method accounts for the intrinsic variability of initiation patterns (Lagarde et al., 2016) and can flexibly adapt to the potential heterogeneities across different seizures of the same patient.

The proposed automated SOZ detection is performed using a two-stage procedure (Fig. 3). First, the most relevant frequency and time windows of interest (the so-called seizure onset windows, SOW) are extracted from the intracranial EEG signals. The algorithm relies on finding time-frequency windows in the transition between pre-ictal and ictal states that yield maximal and spatially confined spectral activations, thus ensuring that propagation has not started and that SOZ contacts can be naturally discriminated from other sites. Then, the most active channels are selected and accumulated over seizures to define the SOZ. The critical step of our analysis is the definition of two measures (Fig. 2), namely the global activation (GA) and the activation entropy (AE), that are later jointly optimized to find the relevant time-frequency window for SOZ localization. On one hand, GA is used to quantify maximal activations with respect to the pre-ictal basal state. Note that in the case where one contact has a very large MA compared to the others, the global activation coincides with the maximum of the MA distribution. However, the robustness of this measure makes it preferable when compared to a summary statistic that takes only one value. On the other hand, the AE is used to characterize how spread spectral activations are across recording sites, independent of the magnitude of these activations, a feature that is strictly measured by GA. To compute the AE, the MA profile is discretized, thus defining a finite number of activation levels. Based on our previous work (Vila-Vidal et al., 2017), we decided to use h = 10 bins to capture the richness of channels' activations.

Although used with the mean activation (MA), the two measures and the optimization procedure that we described here are rather general and can be used in combination with other variables to find spatially confined

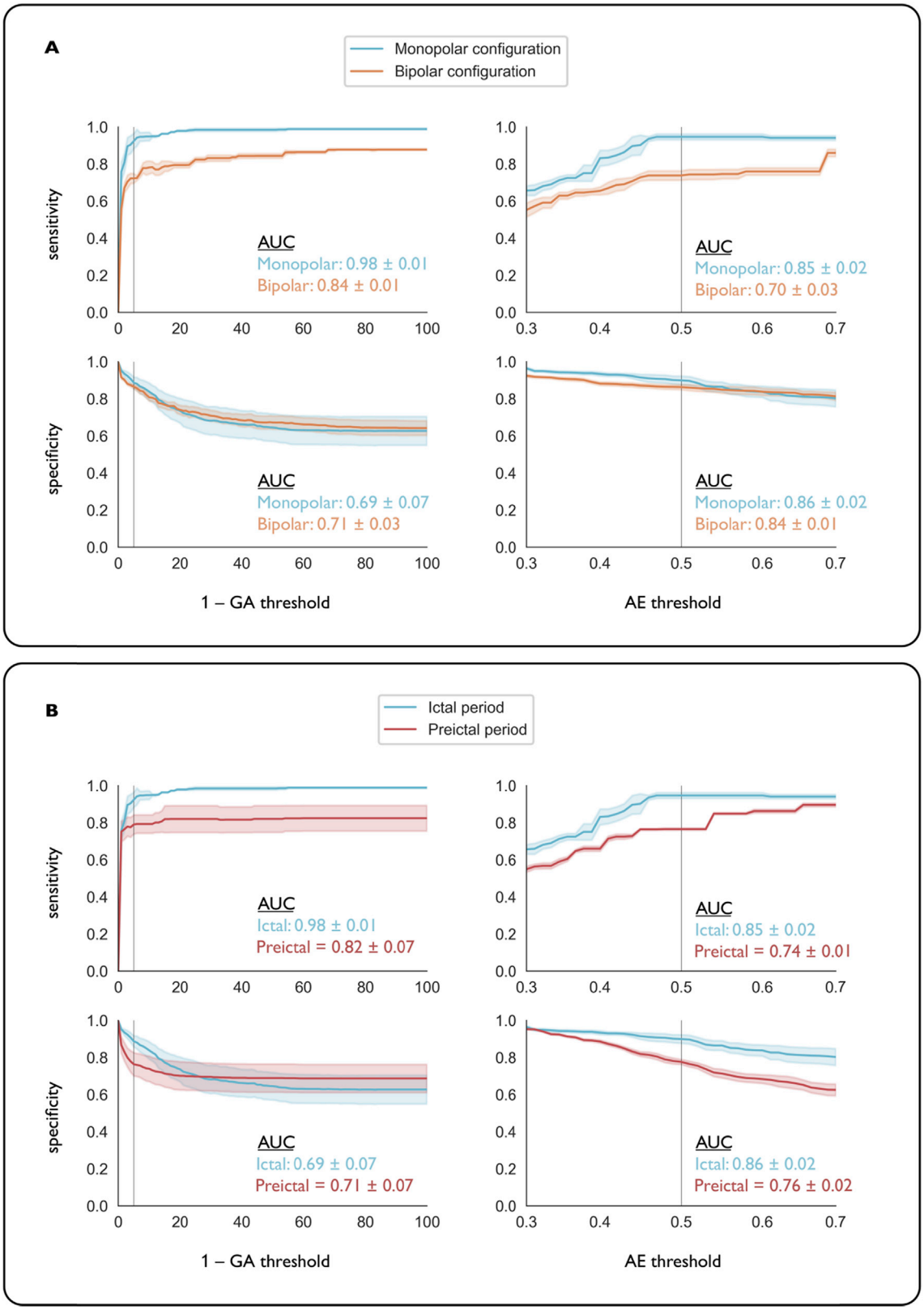

Fig. 6. Patient-average accuracy of the SOZ detection algorithm under different recording configurations and time periods. Because the optimal working point of the detection algorithm might differ under different conditions, a fair comparison across conditions is achieved by computing the accuracy of the algorithm as a function of the threshold values and extracting the area under this curve (AUC) in each condition. The accuracy curves are computed akin to those in Fig. 5B. For each threshold type, the AUC is reported as a fraction of its theoretical maximum (100 and 0.4 for the GA and AE thresholds, respectively). **(A)** Performance comparison between mono- and bipolar referencing. While there is no significant difference in terms of specificity between monopolar and bipolar configurations, the sensitivity of the method is significantly higher in the monopolar configuration. **(B)** Performance comparison between pre-ictal and ictal time periods. Although the method has a better performance in the ictal period, high sensitivities and specificities indicate that the pre-ictal period contains sufficient information for SOZ prediction.

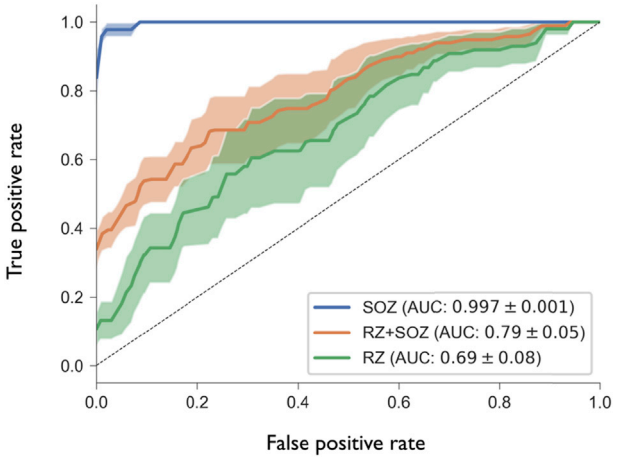

Fig. 7. ROC curves for the prediction of SOZ and RZ regions in Engel I patients. For patients that underwent resective surgery and attained very good post-surgical outcome (Engel I, N = 5 patients), we computed the average nMA over all seizure onset windows, thus obtaining a single nMA index per site. We then computed the ROC curves when using these indices to predict the SOZ, RZ + SOZ and RZ regions, respectively. For each region, the solid line represents the average performance across patients, while the shaded area depicts the standard error of the mean. AUC values are also reported in the figure (mean ± standard error of the mean). The results suggest that the variable nMA carries relevant information for RZ prediction in patients that attained seizure freedom after resective surgery.

events. Specifically, the methodology that we developed may be useful in a number of settings to unravel the characteristic time and frequency scales (pattern signatures) of localized abrupt changes in brain activity during events of interests of both cognitive (e.g. stimuli presentations) and clinical (e.g. brain activity after a stroke) nature.

We have shown that ictal onset is characterized by a general shift towards lower AEs and higher GAs. More specifically, we computed the density of (AE,GA) across seizures in the ictal period and pre-ictal period. A highly populated cluster defined by very high GAs and low AEs could be clearly identified in the ictal epoch. Based on this result, the method finds those windows with maximal global activations (large GA) under the constraint that these activations are spatially confined to a few regions (low AE). These windows are then used to reliably find SOZ sites (Fig. 3). Yet, the specific choice of the thresholds (GA above the 95th percentile and AE<0.5) is rather arbitrary and deserves to be further discussed. We could have used a clustering algorithm to extract the specific boundaries of the dense cluster. However, this would yield more relaxed conditions that would result in a decrease in specificity. Hence, we chose to manually set the thresholds and tune them depending on the desired sensitivity and specificity of the output. Additionally, we did a surrogate analysis and compared the fraction of windows satisfying the required criterion with chance level. This analysis showed a strong correlation between the conditions both in the pre-ictal and ictal periods. We hypothesize that this correlation between very high and spatially confined activations is associated with ictal events and constitutes an *a posteriori* validation of the rationale behind the procedure that we propose. Moreover, a non-negligible consequence of the thresholding step is that seizures where SOZ discrimination cannot be guaranteed with a minimum level of confidence are discarded beforehand, thus ensuring meaningful SOZ detections. Discarded seizures can be further interpreted and might offer complementary insight during the pre-surgical evaluation. Although the treatment of such cases is out of the scope of this study, clinical reviewing of the SEEG recordings from patient 5 showed that the two seizures that had been rejected were indeed preceded by ictal-like activity.

4.2. Clinical relevance of seizure onset windows in terms of ictal patterns

A primary aspect of our analysis is that automatization does not come at the expense of interpretability, as the method provides an output that can be fully read in clinically terms (Fig. 4). As seen in (Lagarde et al., 2016) there is a wide range of seizure onset patterns and while some have a higher prevalence than others, high-frequency discharges cannot be considered to be the only epileptogenic onset biomarker. We have shown that the time-frequency windows selected by the method reliably characterize a variety of electrophysiological seizure onset patterns. In particular, we could isolate the high-amplitude low-frequency spiking activity at 1 Hz that defines the start of the ictal events in one of the analyzed patients.

4.3. Robustness of the method and performance comparison under different conditions

SOZ detection was primarily done in the monopolar setting and using time windows from ictal epochs (Fig. 5A). The average sensitivity across patients was 0.94 ± 0.03, with an average specificity of 0.90 ± 0.03 (mean ± standard error of the mean). SOZ detection was not complete only in three patients (2, 4 and 6) but missed SOZ sites lied at most 1.5 mm apart from the delineated region. We also performed stability analysis on the three parameters of our algorithm (number of bins h, GA threshold and AE threshold) to further validate the theoretical properties backing our parameter choices (Fig. 5B and C). The specificity of the method was found to be minimally dependent on the number of discrete activation levels used to compute the AE. Our choice to use 10 levels was proven effective in capturing the relevant properties of seizure activation, insofar h = 10 lies in a plateau of maximal sensitivities for the SOZ localization problem. We also studied the effect of thresholding the GA and AE quantifiers on the performance of the detection algorithm. The GA threshold (95th percentile) was found to lie at the onset of the sensitivity function stabilization, while in a range of high specificities. On the other hand, the AE threshold (0.5) lies on a plateau of the performance function. As the conditions on GA and AE are relaxed more non-SOZ sites are chosen. Despite being outside the SOZ, we hypothesize that these sites might have a critical role in sustaining and propagating epileptic activity in the early stages of the seizure. Overall, these results constitute a validation of our parameter choices and show the robustness of the method against variations of the parameters values.

Complementary to the main results, we further investigated the effect of the recording referencing on the method performance (Fig. 6A). While no significant differences were found in terms of specificity, the algorithm was more sensitive to SOZ regions in the monopolar configuration. Very few works have assessed the effect of the recording reference on intracranial EEG analysis and they have mainly studied its impact on connectivity measures (Arnulfo et al., 2015). To the best of our knowledge, this is the first study to compare the performance between monopolar and bipolar configurations for SOZ detection. The monopolar referencing yields data contaminated by volume conduction and remote field effects, while the bipolar montage averages out these effects offering a more localized spatial resolution. Yet, we hypothesize that in the case of a partially mapped SOZ, the monopolar configuration might be more sensitive to capture the activity from the missed SOZ sites and thus perform better when used to approximate the focus localization.

Additionally, we chose to explore the performance of the method in a short pre-ictal period (Fig. 6B). Although the method has proven to have a higher performance in the ictal period, the results bring evidence that the pre-ictal period also carries information that might be of interest for SOZ localization, as already seen in previous studies (Andrzejak et al., 2015; Tauste Campo et al., 2018).

Post-operative validation in Engel I patients revealed the potential predictive power of the variable nMA as a biomarker of the resected zone when averaged across seizure onset windows (Fig. 7). This result suggests that the features upon which the method is built characterize the

generation, spread and maintenance of epileptic seizures. Yet, an average predictive value (AUC) for the RZ of 0.69 ± 0.08 (mean ± standard error of the mean) highlights the non-trivial relationship between the SOZ and the whole epileptogenic zone, in line with previous studies (Lüders et al., 2006; Huang et al., 2012; Rummel et al., 2015; Geier et al., 2015).

4.4. Study limitations

The number of patients satisfying sufficiently long post-operative follow-up periods (10) constitutes the major limitation of this study. Further research should be conducted to validate our algorithm with a larger cohort of patients and beyond temporal lobe epilepsy. Additionally, the proposed procedure should be tested in a variety of alternative settings that involve the study of alterations in brain activity that are consistently time-locked to an event (Luck et al., 2000; Lauchaux et al., 2012; Kropotov, 2016).

5. Conclusions

The present study proposes a robust methodology to identify the neural populations undergoing emerging functional or pathological transitions in settings of both experimental and clinical relevance. Our method achieved very high accuracy values when used to predict seizure onset zone regions from peri-ictal SEEG recordings in focal epilepsy. Although our primary analysis relies on the detection of the seizure onset time defined by the clinical neurophysiologists, we have shown that our GA quantifier has the power to automatically predict seizure onset times.

Overall, the proposed procedure could be used to extract the pattern signatures and spatial localization of the brain response to events of interest in a variety of settings of both clinical and cognitive relevance. For example, in finding the brain sites that respond to electrical stimulation or to drug administration, in the analysis of the brain reaction to cognitive stimuli during a task paradigm, in studying the increase in connectivity between distant regions when a stimulus is delivered, etc. In particular, our framework could be easily integrated as a complementary diagnostic tool with minimal computational costs for surgical planning, reducing time-consuming SEEG revisions and improving the clinician decision after pre-surgical evaluation.

Declaration of competing interest

The authors declare no competing financial interests.

Acknowledgments

M.V was supported by a fellowship from ”la Caixa” Foundation, Spain (ID 100010434, fellowship code LCF/BQ/DE17/11600022). G.D. was supported by the Spanish Ministry of Economy and Competitiveness, Spain (grant agreement number PSI2016-75688-P, MINECO/AEI/FEDER-EU); European Union’s Horizon 2020 FET Flagship Human Brain Project (grant agreement number 785907, HBP SGA2); the Catalan Agency for Management of University and Research Grants, Spain (grant agreement number 2017 SGR 1545), and the Swiss National Science Foundation, Switzerland (grant agreement number CRSII5_170873). We thank Mar Moya Giménez for her contribution to the initial stages of this work.

Appendix A. Supplementary information

Supplementary information to this article can be found online at https://doi.org/10.1016/j.neuroimage.2019.116410.

References

Andrzejak, R.G., David, O., Gnatkovsky, V., Wendling, F., Bartolomei, F., Francione, S., et al., 2015. Localization of epileptogenic zone on pre-surgical intracranial EEG recordings: toward a validation of quantitative signal analysis approaches. Brain Topogr. 28 (6), 832–837.

Arnulfo, G., Hirvonen, J., Nobili, L., Palva, S., Palva, J.M., 2015. Phase and amplitude correlations in resting-state activity in human stereotactical eeg recordings. Neuroimage 112, 114–127.

Bartolomei, F., Chauvel, P., Wendling, F., 2008. Epileptogenicity of brain structures in human temporal lobe epilepsy: a quantified study from intracerebral EEG. Brain 131 (7), 1818–1830.

Bourdillon, P., Isnard, J., Chatenoix, H., et al., 2017. Stereo electroencephalography–guided radiofrequency thermocoagulation (SEEG-guided RF-TC) in drug-resistant focal epilepsy: Results from a 10-year experience. Epilepsia 58 (1), 85–93.

David, O., Blauwblomme, T., Job, A.S., Chabardès, S., Hoffmann, D., Minotti, L., et al., 2011. Imaging the seizure onset zone with stereo-electroencephalography. Brain 134 (10), 2898–2911.

Engel, A.K., Moll, C.K., Fried, I., Ojelmann, G.A., 2005. Invasive recordings from the human brain: clinical insights and beyond. Nat. Rev. Neurosci. 6 (1), 35–47.

Geertsema, E.E., Visser, G.H., Velis, D.N., Claus, S.P., Zijlmans, M., Kalitzin, S.N., 2015. Automated seizure onset zone approximation based on nonharmonic high-frequency oscillations in human interictal intracranial eegs. Int. J. Neural Syst. 25 (05), 1550015.

Geier, C., Bialonski, S., Elger, C.E., Lehnertz, K., 2015. How important is the seizure onset zone for seizure dynamics? Seizure 25, 160–166.

Gnatkovsky, V., Francione, S., Cardinale, F., Mai, R., Tassi, L., Lo Russo, G., et al., 2011. Identification of reproducible ictal patterns based on quantified frequency analysis of intracranial EEG signals. Epilepsia 52 (3), 477–488.

Gnatkovsky, V., de Curtis, M., Pastori, C., Cardinale, F., Lo Russo, G., Mai, R., et al., 2014. Biomarkers of epileptogenic zone defined by quantified stereo-EEG analysis. Epilepsia 55 (2), 296–305.

Guenot, M., Isnard, J., Ryvlin, P., Fischer, C., Ostrowsky, K., Mauguiere, F., et al., 2002. Neurophysiological monitoring for epilepsy surgery: the Talairach SEEG method. Stereotact. Funct. Neurosurg. 77 (1–4), 29–32.

Hinkley, D., 1971. Inference about the change point from cumulative sum-tests. Biometrika 58 (3), 509–523.

Huang, C., Marsh, E.D., Ziskind, D.M., Celix, J.M., Peltzer, B., Brown, M.W., et al., 2012. Leaving tissue associated with infrequent intracranial EEG seizure onsets is compatible with post-operative seizure freedom. J. Pediatr. Epilepsy 1 (04), 211–219.

Kropotov, J.D., 2016. Functional Neuromarkers for Psychiatry: Applications for Diagnosis and Treatment. Academic Press.

Lachaux, J.P., Axmacher, N., Mormann, F., Halgren, E., Crone, N.E., 2012. High-frequency neural activity and human cognition: past, present and possible future of intracranial EEG research. Prog. Neurobiol. 98 (3), 279–301.

Lagarde, S., Bonini, F., McGonigal, A., Chauvel, P., Gavaret, M., Scavarda, D., et al., 2016. Seizure-onset patterns in focal cortical dysplasia and neurodevelopmental tumors: relationship with surgical prognosis and neuropathologic subtypes. Epilepsia 57 (9), 1426–1435.

Liu, S., Sha, Z., Sencer, A., Aydoseli, A., Bebek, N., Abosch, A., et al., 2016. Exploring the time–frequency content of high frequency oscillations for automated identification of seizure onset zone in epilepsy. J. Neural Eng. 13 (2), 026026.

Luck, S.J., Woodman, G.F., Vogel, E.K., 2000. Event-related potential studies of attention. Trends Cogn. Sci. 4 (11), 432–440.

Lüders, H.O., Najm, I., Nair, D., Widdess-Walsh, P., Bingman, W., 2006. The epileptogenic zone: general principles. Epileptic Disord. 8 (2), 1–9.

Munari, C., Bancaud, J., 1985. The role of stereo-EEG in the evaluation of partial epileptic seizures. In: Porter, R.J., Morselli, P.L. (Eds.), The Epilepsies. Butterworths, London, pp. 267–306.

Murphy, P.M., von Paternos, A.J., Santaniello, S., 2017. A novel HFO-based method for unsupervised localization of the seizure onset zone in drug-resistant epilepsy. In: Engineering in Medicine and Biology Society (EMBC), 2017 39th Annual International Conference of the IEEE. IEEE, pp. 1054–1057.

Page, E., 1954. Continuous inspection schemes. Biometrika 41, 100–115.

Perucca, P., Dubeau, F., Gotman, J., 2014. Intracranial electroencephalographic seizure-onset patterns: effect of underlying pathology. Brain 137 (1), 183–196.

Rummel, C., Abela, E., Andrzejak, R.G., Hauf, M., Pollo, C., Müller, M., et al., 2015. Resected brain tissue, seizure onset zone and quantitative EEG measures: towards prediction of post-surgical seizure control. PLoS One 10 (10), e0141023.

Talairach, J., Bancaud, J., Szikla, G., Bonis, A., Geier, S., Vedrenne, C., 1974. New approach to the neurosurgery of epilepsy. Stereotaxic methodology and therapeutic results. 1. introduction and history. Neurochirurgie 20 (Suppl. 1), 1–240.

Tauste Campo, A., Principe, A., Ley, M., Rocamora, R., Deco, G., 2018. Degenerate time-dependent network dynamics anticipate seizures in human epileptic brain. PLoS Biol. 16 (4), e2002580.

Varatharajah, Y., Berry, B.M., Kalbarczyk, Z.T., Brinkmann, B.H., Worrell, G.A., Iyer, R.K., 2017. Inter-ictal seizure onset zone localization using unsupervised clustering and bayesian filtering. In: Neural Engineering (NER), 2017 8th International IEEE/EMBS Conference on. IEEE, pp. 533–539.

Vila-Vidal, M., Principe, A., Ley, M., Deco, G., Tauste Campo, A., Rocamora, R., 2017. Detection of recurrent activation patterns across focal seizures: application to seizure onset zone identification. Clin. Neurophysiol. 128 (6), 977–985.